Carlson, K.D., and Beckermann, C., "Prediction of Riser Carbon Macrosegregation due to Shrinkage Flow in Steel Casting," in Proceedings of the 64th SFSA Technical and Operating Conference, Paper No. 3.2, Steel Founders' Society of America, Chicago, IL, 2010.

# Prediction of Riser Carbon Macrosegregation due to Shrinkage Flow in Steel Casting

**Kent D. Carlson and Christoph Beckermann**[1]

**Department of Mechanical and Industrial Engineering**

**The University of Iowa, Iowa City, IA 52242**

## Abstract

A new simulation model is developed that predicts carbon macrosegregation in and below risers due to feeding flow in steel castings. The model uses feeding flow velocities predicted with a new advanced feeding flow model that predicts melt pressure, feeding flow and porosity formation and growth during casting solidification. These new models are utilized to simulate carbon macrosegregation in three experimental top-risered cube castings (one with no breaker core, one with a 75% breaker core, and one with a 50% breaker core), that were cast to study under-riser carbon macrosegregation. The simulated and experimental results for these castings are compared. Positive carbon macrosegregation in all three risers is predicted reasonably well, indicating that feeding flow is the driving force behind macrosegregation in the riser. The carbon concentration is reasonably well predicted in the under-riser region of the casting with no breaker core, in which significant under-riser macrosegregation does not occur. In both breaker core castings, a region of positive macrosegregation is predicted in the cube beneath the riser, as seen in the experiments. This indicates that feeding flow is an important consideration in determining under-riser macrosegregation. However, the predicted magnitudes and locations of these positive under-riser macrosegregation regions are at best only qualitatively correct, which indicates that natural convection (which is not considered in the present model) plays an important role in under-riser carbon macrosegregation, in addition to feeding flow.

[1] Author to whom correspondence should be addressed. Telephone: (319) 335-5681, Fax: (319) 335-5669, E-mail: becker@engineering.uiowa.edu

## 1. Introduction

Segregation of alloying elements occurs in virtually all steel casting processes. The root cause of segregation is the fact that most alloying elements are more soluble in the liquid phase than in the solid phase. Thus, as metal solidifies, alloying elements in the mushy zone (solidifying liquid-solid mixture) are rejected from the growing solid dendrites into the neighboring interdendritic liquid, which becomes more and more enriched with alloying elements as solidification proceeds. On the scale of the dendrites (tens to hundreds of microns), segregation results in a non-uniform solute distribution in and between the dendrite arms. This is termed microsegregation. Considering a small volume element containing many dendrites and the liquid between them, the average composition resulting from microsegregation is still the nominal composition, $C_0$. However, if there is relative movement between dendritic solid and interdendritic liquid in the mushy zone, then liquid or solid with a solute concentration different from the nominal composition can move within the solidifying casting, thus changing the average local composition of the solidifying mixture. If this relative movement occurs over large distances (i.e., much larger than the scale of the dendrites), the change that this movement effects in the average local solute concentration away from the nominal composition is termed macrosegregation. Unlike microsegregation, macrosegregation can result in a casting with regions having a composition quite different from the nominal value. If the local composition is above the nominal value, this is termed positive macrosegregation; if the composition is below the nominal value, it is termed negative macrosegregation.[1]

The current study focuses on carbon macrosegregation that commonly occurs beneath risers. This under-riser segregation can cause significant problems in steel casting. First of all, segregated under-riser casting regions may have inferior mechanical properties, because the steel chemistry in this region is different from the intended chemistry. Secondly, under-riser segregation can lead to under-riser cracking in the casting when the riser is removed or when the surface is machined. Insightful discussions regarding the causes and effects of under-riser segregation, as well as common industry practices to prevent it from occurring, can be found in two previous SFSA T&O papers written by Ken Murphy.[2-3]

In the present investigation, a model is developed that predicts macrosegregation caused by shrinkage-driven flow moving from risers into the casting (for example) to feed solidification shrinkage. A species conservation equation is employed that utilizes feeding flow velocities determined using a new advanced feeding model. This new macrosegregation model is used to predict carbon macrosegregation in three simple experimental castings, in which carbon concentrations were measured. The predicted carbon concentration profiles are then compared with the measured values.

It is very important to note that there are several possible causes of macrosegregation that may be relevant in the present study. One is shrinkage-driven flow. Another is buoyancy-driven flow (i.e., natural convection), caused by thermal and/or solutal gradients in the liquid. In addition, macrosegregation may also be caused by solid movement due to the settling of equiaxed grains or solid fragments.[1] Since the present macrosegregation model considers only

shrinkage-driven flow, it can not completely predict macrosegregation. However, by determining where predicted carbon concentrations are in agreement with observed values and where they differ, some light will be shed on which macrosegregation regions are the result of shrinkage-driven flow, and which regions are the result of other causes.

In the next section, the experimental casting results utilized in this study will be discussed. Then, the advanced feeding and macrosegregation models will be presented. This will be followed by a description of the casting simulations and presentation of the simulated macrosegregation results. Finally, the predicted and measured carbon macrosegregation values will be compared.

## 2. Experimental Castings

Under-riser carbon macrosegregation was studied experimentally many years ago by American Cast Iron Pipe Company (formerly known as ACIPCO, presently known simply as AMERICAN).[2,4] A series of ten inch cube castings, with a variety of riser arrangements, were cast using AISI 1035 steel in green sand molds. The measured alloy composition in the ladle was 0.360% C, 0.76% Mn, 0.028% P, 0.020% S, and 0.048% Al. The present study considers three of these castings, shown schematically in Fig. 1. All three castings considered here utilized 8 in. diameter, 9.4 in. high risers with mildly exothermic-insulating sleeves and hot topping. In the first casting (Fig. 1a), the riser was placed directly on top of the cube. For the second and third castings (Figs. 1b and 1c), 1 in. thick breaker cores were inserted between the cube and the riser. The second casting (Fig. 1b) used a 6 in. diameter (i.e., 75%) breaker core, while the third casting (Fig. 1c) used a 4 in. diameter (i.e., 50%) breaker core.

In order to analyze the carbon concentrations in these castings, slabs were cut from the center of each casting, and the mid-casting face of each slab was etched with 10% nitric acid to reveal carbon macrosegregation. The etched slab from the casting without a breaker core is shown in Fig. 2c. The dark areas in this picture correspond to positive carbon macrosegregation. It is seen that positive macrosegregation is mostly confined within the riser. The dark, thin diagonal lines seen near the top corners of the cube (particularly visible on the left side of the cube) correspond to “A” segregates.[1] The slabs were then drilled in various locations to measure the carbon content, as shown in Fig. 2a (no breaker core), Fig. 3a (75% breaker core) and Fig. 4a (50% breaker core). The carbon values determined from this process are printed on the castings next to their corresponding locations. Note that no photographs are available of the etched slabs from the two breaker core castings prior to drilling, but the etching in these two castings is visible in Figs. 3a and 4a. Fig. 3a shows positive macrosegregation in the riser, the riser neck, and in the under-riser region of the cube with a 75% breaker core. Fig. 4a shows positive macrosegregation in the riser and in the upper portion of the cube with a 50% breaker core. Both Figs. 3a and 4a also show evidence of “A” segregates in the cubes. Comparing Figs. 2c, 3a and 4a, it is clear that the central region of positive carbon macrosegregation moves down from the riser into the cube as the riser neck size decreases.

The vertical centerline carbon measurements for all three castings are plotted together in Fig. 5 as a function of the distance from the bottom of the castings. Vertical lines indicate the top of the cube, the neck region (for the castings with a breaker core), and the riser. The carbon concentrations are normalized by the measured ladle carbon content ($C_0 = 0.36\%$) to give the carbon index (see Section 3.2 for more on the carbon index). All three castings show the same macrosegregation trend in the riser: starting at the bottom of the riser, the carbon index increases moving up the riser. The casting with no breaker core and the casting with a 75% breaker core both exhibit positive macrosegregation (i.e., carbon index > 1) throughout the riser. The casting with a 50% breaker core has negative macrosegregation (i.e., carbon index < 1) at the bottom of the riser where it connects to the riser neck, and then increases moving up the riser. The highest measurement in the 50% breaker core casting displays negative macrosegregation. Considering Fig. f4a, notice that the highest drilling in the 50% breaker core casting appears to be in the vicinity of the riser pipe; there is riser pipe-related porosity immediately to the right of this drilling, both above and below the drilling. Also notice that there are dark etched regions above and to the right of the drilling, indicating positive macrosegregation. This figure indicates the sensitivity to location of the measured carbon concentrations near the riser.

Returning to the discussion of Fig. 5, it is seen that the positive macrosegregation in the riser of the casting with no breaker core originates close to the top of the cube, and that there is essentially no macrosegregation in the under-riser region beneath this. In each of the breaker core castings, however, notice that there is significant positive macrosegregation in the under-riser region of the cube. Also note that the location of the maximum positive macrosegregation (which roughly indicates the middle of this positive macrosegregation region) moves lower in the cube as the breaker core size decreases. Finally, notice that the change in the macrosegregation profiles is not of a predictable, monotonic nature as the breaker core size decreases. In the under-riser and riser regions, the 75% breaker core macrosegregation profile displays more positive macrosegregation at every location than the casting with no breaker core. When the breaker core size decreases to 50%, the trend of increasing positive macrosegregation in the under-riser region continues, but the carbon index drops suddenly in the riser neck, resulting in negative macrosegregation at the top of the riser neck rather than positive. This results in the carbon index in the riser of the 50% breaker core casting being smaller at every location than in either of the other castings.

## 3. Numerical Modeling of Feeding Flow and Carbon Macrosegregation

The primary focus of the present investigation is the carbon macrosegregation model. However, this model uses feeding flow velocities determined by the advanced feeding model, so it is beneficial to briefly describe the advanced feeding model to provide context for the macrosegregation model. Additionally, the riser pipe, which is also predicted by the advanced feeding model, warrants discussion because it plays a role in the final segregation profile. Therefore, this section will first describe the advanced feeding model, including riser pipe formation. Afterward, the macrosegregation model will be presented. Finally, the implementation of these models will be briefly described.

3.1 Advanced Feeding Model

The macrosegregation model utilizes feeding flow velocities predicted by the new advanced feeding model.[5-6] The advanced feeding model determines melt pressure, feeding flow, and shrinkage porosity formation and growth during casting solidification. This is accomplished by solving mixture mass conservation and liquid momentum conservation equations that are derived assuming an averaging volume composed of some combination of solid metal $(s)$, liquid metal $(l)$, and porosity $(p)$, such that the volume fractions of these three phases satisfy the relation: $g_s + g_l + g_p = 1$. Mixture properties are determined by the sum of the property values of each phase multiplied by their respective volume fractions. For example, the mixture density is given by: $\rho = g_s\rho_s + g_l\rho_l + g_p\rho_p$. Note that for pure shrinkage porosity, with no dissolved gases in the melt, the pore pressure ($P_p$) and pore density ($\rho_p$) are negligibly small, due only to vapor pressure of the elements in the melt. Therefore, and the mixture density simplifies to: $\rho = g_s\rho_s + g_l\rho_l$. Assuming that the solid and porosity phases are stationary, the mixture mass conservation equation and the liquid momentum conservation equation can then be expressed as:

$$\text{Mass: } \frac{\partial}{\partial t}\left(g_s\rho_s + g_l\rho_l\right) + \nabla\cdot\left(g_l\rho_l\overline{v}_l\right) = 0 \tag{1}$$

$$\text{Momentum: } \nabla^2\left(g_l\overline{v}_l\right) = \frac{g_l}{K}\left(g_l\overline{v}_l\right) + \frac{g_l}{\mu_l}\nabla P - \frac{g_l}{\mu_l}\rho_{l,ref}\,\overline{g} \tag{2}$$

where $\overline{v}_l$ is the intrinsic velocity; $P$ is the melt pressure; the subscripts $s$, $l$ and $p$ indicate the phase; $g$ is the volume fraction; $\rho$ is the density; $\rho_{l,ref}$ is the reference liquid density, taken as the melt density at the liquidus temperature; $\mu_l$ is the liquid dynamic viscosity, $K$ is the permeability of the solidifying metal; $\overline{g}$ is the gravity vector; and $t$ is the time. Neglecting the surface tension at the pore-liquid interface, shrinkage porosity forms in solidifying metal when the local melt pressure drops to zero (i.e., vacuum). This porosity then grows with the local melt pressure fixed to zero to satisfy Eq. (1), substituting $g_l = 1 - g_s - g_p$, until solidification is complete. The advanced feeding model is described in more detail in Refs. [5-6].

The formation of the riser pipe due to solidification shrinkage is also considered in the advanced feeding model. The motion of the metal free surface of the riser pipe is tracked using a VOF-type method, by solving the following mass conservation equation for air:

$$\frac{\partial g_a}{\partial t} + \nabla\cdot\left(g_a\overline{u}_a\right) = 0 \tag{3}$$

where $g_a$ is the air fraction ($g_s + g_l + g_p + g_a = 1$ in riser pipe regions containing a free surface), and $\overline{u}_a$ is the air velocity. This surface tracking method is employed at locations along

the riser pipe free surface where the melt pressure is less than or equal to the ambient pressure, provided that the liquid fraction at the location under consideration is greater than or equal to a critical value, $g_{l,cr}$. If the liquid fraction is smaller than this critical value, it is assumed that the dendritic network is sufficient to prevent the surface from moving. When these two conditions ($P \le P_{amb}$ and $g_l \ge g_{l,cr}$) are met at a location on the riser pipe free surface, the local melt pressure is forced to the value $P_{amb}$, and Eq. (3) is solved to determine the position of the free surface by determining the air fraction, $g_a$.

3.2 Carbon Macrosegregation Model

The carbon concentration throughout the solidifying casting is determined by solving the following species conservation equation, which assumes there is no carbon in the porosity or air phases:

$$g_l \rho_l \frac{\partial C_l}{\partial t} + g_l \rho_l \overline{v}_l \cdot \nabla C_l = -g_s \rho_s \frac{\partial C_s}{\partial t} + \left(C_l - C_s\right) \frac{\partial}{\partial t}\left(g_s \rho_s\right) \tag{4}$$

where $C_l$ and $C_s$ are the carbon concentrations in the liquid and solid phases, respectively, and $\overline{v}_l$ is determined by solving Eqs. (1) and (2). Carbon is a fast-diffusing element, and hence $C_s$ is modeled using the lever rule, which gives

$$C_s = \kappa C_l \tag{5}$$

where $\kappa$ is the carbon partition coefficient. Combining Eqs. (4) and (5), the conservation equation for carbon can be written as:

$$g_l \rho_l \frac{\partial C_l}{\partial t} + g_l \rho_l \overline{v}_l \cdot \nabla C_l = -g_s \rho_s \frac{\partial}{\partial t}\left(\kappa C_l\right) + C_l\left(1 - \kappa\right) \frac{\partial}{\partial t}\left(g_s \rho_s\right) \tag{6}$$

Initial and boundary conditions are necessary in order to solve Eq. (6). Initially, the carbon concentration throughout the casting is assumed to be equal to the initial concentration, which is expressed as $C_l = C_0$. At the casting surfaces, a zero gradient condition is imposed, or $\partial C_l / \partial n = 0$, where $n$ is the direction normal to the boundary. Using these conditions, Eq. (6) can be solved to determine the carbon concentration in the liquid throughout the casting, and Eq. (5) can be solved to find the carbon concentration in the solid. These quantities can be combined into a mixture concentration, $C_{mix}$:

$$C_{mix} = \frac{g_s \rho_s C_s + g_l \rho_l C_l}{g_s \rho_s + g_l \rho_l} \tag{7}$$

Finally, Eq. (7) can be normalized by the initial concentration, $C_0$, to give a quantity termed the macrosegregation index or carbon index:

$$\text{carbon index} = \frac{C_{mix}}{C_0} = \frac{\left(g_s \rho_s C_s + g_l \rho_l C_l\right)}{C_0 \left(g_s \rho_s + g_l \rho_l\right)} \tag{8}$$

Note that when the casting is completely solidified (i.e., $g_l = 0$), the carbon index given by Eq. (8) reduces to $C_s / C_0$, the normalized carbon concentration in the solidified casting.

Finally, while the current focus is on carbon macrosegregation, Eq. (6) is applicable for any fast-diffusing element (C, N, etc.). An expression similar to Eq. (6) can be derived for slow-diffusing elements, replacing the lever rule in Eq. (5) with the following Scheil equation:

$$\frac{\partial}{\partial t}\left(g_s \rho_s C_s\right) = \kappa C_l \frac{\partial}{\partial t}\left(g_s \rho_s\right) \tag{9}$$

Eq. (9) can be combined with Eq. (4) to develop a conservation equation for any slow-diffusing element, analogous to Eq. (6). This yields:

$$g_l \rho_l \frac{\partial C_l}{\partial t} + g_l \rho_l \overline{v}_l \cdot \nabla C_l = C_l \left(1 - \kappa\right) \frac{\partial}{\partial t}\left(g_s \rho_s\right) \tag{10}$$

Thus, the concentration of any alloying element throughout the casting can be determined with this model, utilizing Eq. (6) for each fast-diffusing element and Eq. (10) for each slow-diffusing element.

### 3.3 Implementation of Models

The advanced feeding and macrosegregation models described above are implemented as special models within the commercial casting simulation software package MAGMAsoft.[7] During solidification, the temperature field is determined using the standard MAGMAsoft solidification module. This temperature data is then utilized to determine the temperature-dependent material properties needed to solve Eqs. (1) and (2) for the feeding velocities, and then to solve Eq. (6) for the carbon concentration in the liquid. Once the liquid concentration is determined, the solid concentration can be found from Eq. (5), and the carbon index can be calculated using Eq. (8).

## 4. Feeding Flow and Carbon Macrosegregation Simulations

The AISI 1035 property dataset required to simulate the solidification of the three experimental castings described in Section 2 was generated using the interdendritic solidification package IDS.[8] The dataset was created using the chemistry provided in Section 2, with a constant cooling rate of 0.1°C/s. The temperature-dependent carbon partition coefficient curve generated by IDS is shown in Fig. 6. Notice the sharp increase in this coefficient at about 1489°C, which corresponds to the rapid transformation of the solidifying metal from ferrite to austenite at this temperature. Before this transformation occurs, carbon is more than five times less soluble in the solid than in the liquid. After the transformation, carbon is about three times less soluble in the solid than in the liquid.

Solidification of the experimental castings was simulated using MAGMAsoft. Filling was not simulated. The initial temperature was taken to be 1565°C (about a 60°C superheat). For each of the three castings, the sand mold was modeled using MAGMA's green sand database (GREEN_SAND). Foseco databases were used to model the properties of the exothermic riser sleeve (KALMINEX_35) and the breaker core (BC_Silica). A constant heat transfer coefficient of 1000 W/m$^2$-K was used between the metal and the sand mold, and between the metal and the breaker core. Temperature-dependent heat transfer coefficients from the Foseco database were used to model the heat transfer between the sleeve and breaker core and the materials with which they are in contact. The hot topping was modeled by simply defining each riser as open, which prompts MAGMAsoft to apply its default hot topping heat transfer boundary condition. For the riser pipe model described in Section 3.1, the default critical liquid value ( $g_{l,cr} = 0.65$ ) was used. A uniform 5 x 5 x 5 mm grid was employed, which resulted in about 190,000 casting control volumes in each simulation.

Fig. 7 shows velocity vectors at the casting mid-plane during the solidification of each casting. Fig. 7a shows a view of the entire casting without a breaker core, to illustrate the location of the cube-riser junction region that is shown in Figs. 7b – 7d. The color contours provide the temperature distribution, where the minimum and maximum temperatures on the scale are the solidus and liquidus temperatures, respectively. Fig. 7b shows the cube-riser junction region for the casting without a breaker core, while Figs. 7c and 7d show the same region for the 75% breaker core and 50% breaker core castings, respectively. Two horizontal lines are included to highlight the velocity profiles at the top of each cube as the metal flows downward from the riser into the cube. As indicated in each figure, a velocity vector beginning at the top line and ending at the bottom line has a magnitude of 40 $\mu$m/s, or 0.040 mm/s. For the casting without a breaker core (Fig. 7b), the maximum velocity is about 30 $\mu$m/s, and the velocity decreases rapidly to the right of the maximum value as the temperature decreases. Figs. 7c and 7d indicate that as the riser neck size decreases, the velocities entering the cube increase. This is reasonable, because the amount of feed metal required by each casting is about the same, and to provide the same volumetric flow rate of feed metal into each cube, the velocity must increase as the casting area through which metal flows into the cube decreases. For the 50% breaker core casting in Fig. 7d, the maximum velocity has reached about 40 $\mu$m/s, and the velocity remains relatively high across the entire neck.

The mid-plane porosity results predicted by the advanced feeding algorithm for each of the three castings are shown in Figs. 2b, 3b and 4b. As expected, the porosity results indicate that the only significant shrinkage porosity present in these castings is located in the riser pipes. Unlike riser pipes generated with the traditional MAGMAsoft feeding algorithm, which transition rapidly from sound metal to empty riser pipe regions, the advanced feeding algorithm produces riser pipes with porosity values that transition more slowly from sound metal to empty riser pipe. The riser pipes for each of the three castings are all very similar, with high porosity values in the top third of the risers, and small amounts of porosity extending down to an inch or two above the bottom of the risers. It is quite reasonable that the porosity predictions are all similar, because

about the same amount of feed metal is required in each casting, and the cooling rates throughout solidification are similar for all three castings.

The mid-plane carbon index values predicted by the macrosegregation simulations are shown in Figs. 2d, 3c and 4c. The purple contour regions in each figure indicate the regions where the carbon index is approximately one (0.99 – 1.01), indicating no macrosegregation. These three figures are re-plotted together in Fig. 8, in order to observe the predicted changes in carbon concentration as the riser neck size decreases. Each casting has a similar region of high carbon index in the riser, just below the riser pipe region, with relatively large carbon index values. In the casting without a breaker core (Fig. 8a), negligible macrosegregation is seen in the under-riser region of the cube. For the 75% (Fig. 8b) and 50% (Fig. 8c) breaker core castings, negative macrosegregation is predicted in the riser neck, and a region of positive macrosegregation is predicted below this in the under-riser region of the cube. The magnitudes of the negative macrosegregation in the riser neck and the positive macrosegregation in the under-riser region both increase as the breaker core size decreases.

Finally, the results in Fig. 8 are compared further in Fig. 9, plotting the carbon index values along the vertical centerline of each of these castings, analogous to Fig. 5 for the experimental castings. Fig. 9 illustrates that, for all three castings, positive macrosegregation is predicted in each riser beginning near the bottom, with the magnitude increasing sharply moving up the riser. Each carbon index curve increases to a maximum (corresponding to the center of the high carbon index region seen in the risers in Fig. 8), and then decreases again above this. The maximum value seen in each riser decreases slightly as the riser neck size decreases, but otherwise these curves are very similar. The shift in the location of the maximum seen in the curve for the casting with no breaker core is simply due to the fact that the riser for this casting starts an inch below the breaker core castings (since there is no breaker core), and hence the top of the riser in this casting is an inch shorter than in the breaker core castings. In the under-riser region of the casting with no breaker core, very little macrosegregation is evident. However, in each breaker core casting, significant positive macrosegregation is seen in the under-riser region of the cube. The magnitude of this positive macrosegregation increases as the breaker core size decreases. Similarly, each breaker core casting also has a region of significant negative macrosegregation in and slightly below the riser neck, which increases in magnitude as the breaker core size decreases.

## 5. Comparison Between Simulation and Experimental Results

The simulation results in Figs. 2 – 4 are presented next to photographs of each casting so that the results predicted by the simulations can be compared to the corresponding experimental results. First, compare the observed riser pipes in Figs. 2a, 3a and 4a with the riser pipe predictions shown in the simulated porosity plots in Figs. 2b, 3b and 4b. The shapes of the completely empty parts on top of each riser pipe seem to be reasonably represented by the regions of high porosity in the simulation results. Comparing the lower parts of the observed riser pipes, where shrinkage holes are visible in metal, it is seen that all regions containing visible holes appear in areas where porosity is predicted, and that these holes extend down to

regions where the porosity prediction is relatively low (< 10%). Overall, the porosity predictions seem reasonable compared to the observed riser pipes. A final note concerning the shape (i.e., shallowness/steepness) of the riser pipe: changing the critical liquid fraction value in the riser pipe model (see Section 3.1) from the default value of $g_{l,cr} = 0.65$ would change the shape of the riser pipe; this was not investigated in the present study, as the present riser pipe predictions seem reasonable.

Carbon macrosegregation results are also compared in Figs. 2 – 4. For all three castings, good qualitative agreement is seen between the observed regions of positive macrosegregation in the risers (Figs. 2c, 3a and 4a) and the predicted high carbon index values in the corresponding risers (Figs. 2d, 3c and 4c). The variations in carbon level corresponding to the "A" segregates seen in the cubes in Figs. 2c, 3a and 4a are not predicted by the simulations because "A" segregates are caused by buoyancy that is induced by solutal gradients, and buoyancy-driven flow is not considered in the present model. For the casting with no breaker core, positive macrosegregation is not seen in the under-riser region of the cube (Fig. 2c), and this is reflected in the prediction (Fig. 2d). For the 75% breaker core casting, the positive macrosegregation observed in Fig. 3a persists down through the riser neck and into the top of the cube, whereas the simulation predicts a region of negative macrosegregation in the neck and in the top of the cube before returning to positive macrosegregation in the under-riser region of the cube. Finally, for the 50% breaker core casting, the etched casting in Fig. 4a shows positive under-riser macrosegregation beginning in the middle of the neck, and continuing down into the top portion of the cube. The simulated carbon index results in Fig. 4c correctly predict a positive under-riser macrosegregation region, but it begins further down in the cube compared to Fig. 4a.

To further compare the predicted and measured segregation results, the measured vertical centerline carbon index values shown in Fig. 5 are compared to the corresponding simulated carbon index values shown in Fig. 9. The predicted and measured values for the casting without a breaker core are compared in Fig. 10. The agreement throughout this casting is reasonably good. Both the prediction and the measurement show increasingly positive macrosegregation in the riser, beginning near the top of the cube, with no significant macrosegregation in the under-riser region of the cube. The simulated carbon index in the riser begins to decrease above a certain point near the simulated riser pipe. As mentioned earlier, this decrease would also be expected in the measurements if it were possible to take them higher in the riser. The discrepancy in carbon index near the riser pipe is due to minor differences in the observed and simulated riser pipes, and displays the sensitivity of macrosegregation to the proximity of the riser pipe. The comparison for the 75% breaker core casting is provided in Fig. 11. Qualitative agreement is seen between the simulated and measured trend in the riser of positive, increasing macrosegregation, as in the casting with no breaker core, although the magnitude of positive macrosegregation is under-predicted. Furthermore, the measured macrosegregation in the riser neck is significantly positive, whereas the simulation predicts mild negative macrosegregation in the neck. A region of positive macrosegregation is predicted in the under-riser region of the cube, but it is somewhat lower than the observed positive macrosegregation region. Finally, the comparison for the 50% breaker core casting is given in Fig. 12. For this casting, the correct

trend is seen throughout the riser, with negative macrosegregation at the bottom of the riser, increasing with height through the riser, and then falling again near the riser pipe. Although the negative macrosegregation at the top of the riser neck is somewhat under-predicted, good agreement is seen in the measured and predicted values in the bottom of the riser. The difference in the location of the maximum values in the riser are again due to differences between the measured and predicted riser pipes. In the under-riser region of the cube, the simulation again correctly predicts a region of positive macrosegregation. However, the magnitude and size of this region are both under-predicted.

The comparisons in Figs. 10 – 12 provide valuable information about the mechanisms that are responsible for the carbon macrosegregation seen in the experimental castings. In the risers, the measured positive carbon macrosegregation is predicted reasonably well, which indicates that feeding flow is indeed the driving force behind macrosegregation in the risers. In the two breaker core castings, the positive macrosegregation seen in the under-riser region of the cubes is predicted, indicating that feeding flow is indeed an important consideration in under-riser macrosegregation. However, the predictions in these under-riser regions are not in particularly good agreement with the measured values; agreement is only qualitative at times, and the locations of the positive under-riser macrosegregation regions are not quite correct. This indicates that buoyancy-driven flow is important in these regions, and that both feeding flow and buoyancy-driven flow must be considered in order to correctly predict the macrosegregation profiles seen in these regions of the experimental castings.

## 6. Conclusions

A new simulation model has been developed that predicts carbon macrosegregation due to feeding flow in steel castings. The model uses feeding flow velocities predicted with a new advanced feeding flow model that predicts melt pressure, feeding flow and porosity formation and growth during casting solidification. These new models were employed in the present study to simulate the solidification of three experimental cube castings that were produced to study under-riser carbon macrosegregation, and the simulation results were compared to measurements and observations in the experimental castings. The riser pipes predicted with the new advanced feeding model are in reasonably good agreement with the riser pipes observed in the castings. Also, positive carbon macrosegregation seen in all three risers is predicted fairly well. For the casting without a breaker core, no significant under-riser macrosegregation occurs, and the simulation predicts this correctly. In both breaker core castings, a region of positive macrosegregation is predicted in the cube beneath the riser, as seen in the experiments. Furthermore, the magnitude of the positive macrosegregation increases as the breaker core size decreases, which is in agreement with what is seen in the measurements. The predicted under-riser macrosegregation results for the casting with a 50% breaker core are in qualitative agreement with the measured values, but the predicted region of positive under-riser macrosegregation is not close enough to the neck, and the magnitude of the macrosegregation is under-predicted. The predicted under-riser results for the casting with a 75% breaker core display the poorest agreement with measurements, with the prediction indicating a negative macrosegregation region in the neck, where positive macrosegregation was measured.

Because the simulations performed for this study only predict carbon macrosegregation due to feeding flow, these results shed some light on the cause of the macrosegregation measured in the experimental castings. The trend of positive macrosegregation in the risers appears to be due to feeding flow, since these values are predicted reasonably well by the present macrosegregation model. For both breaker core castings, the regions of positive macrosegregation beneath the risers observed in the experimental castings are predicted, indicating that feeding flow is an important factor in under-riser macrosegregation. However, discrepancies between the predicted and measured carbon concentrations in the under-riser region indicate that buoyancy-driven flow (i.e., natural convection, which is not considered in the present model) is also important in this region. Thus, in order to correctly predict under-riser carbon macrosegregation in these castings, both feeding flow and buoyancy-driven flow must be taken into account.

**Acknowledgements**

The authors would like to thank Ken Murphy of American Cast Iron Pipe Company, for providing the experimental data used in this study. The authors would also like to thank MAGMA GmbH, for its generous support via donation of software, time and information.

**References**

1. C. Beckermann, "Macrosegregation," in ASM Handbook, Volume 15: Casting, ed. S. Viswanathan, ASM International, Materials Park, OH (2009), pp. 348-352.
2. K.W. Murphy, “Under-Riser Segregation,” *Proc. 39th SFSA Technical and Operating Conference*, Chicago, Illinois (1985).
3. K.W. Murphy, “Understanding Under Riser Cracking," *Proc. 52nd SFSA Technical and Operating Conference*, Chicago, Illinois (1998).
4. W.T. Adams, Jr. and K.W. Murphy, “Optimum Full Contact Top Risers to Avoid Severe Under Riser Chemical Segregation in Steel Castings,” *AFS Trans.*, 88 (1980), pp. 389-404.
5. K.D. Carlson, Z. Lin, R.A. Hardin, C. Beckermann, G. Mazurkevich, and M.C. Schneider, "Modeling of Porosity Formation and Feeding Flow in Steel Casting," *Modeling of Casting, Welding and Advanced Solidification Processes - X*, ed. D.M. Stefanescu et al., (Warrendale, PA: TMS, 2003), pp. 295-302.
6. K.D. Carlson, Z. Lin and C. Beckermann, “Modeling the Effect of Finite-Rate Hydrogen Diffusion on Porosity Formation in Aluminum Alloys,” *Metall. Mater. Trans. B*, 36B (2007), pp. 541-555.
7. MAGMAsoft v4.6, Magma GmbH, Aachen, Germany.
8. J. Miettinen, ”Calculation of Solidification-Related Thermophysical Properties for Steels,” *Metall. Trans. B*, 28B (1997), pp. 281-297.

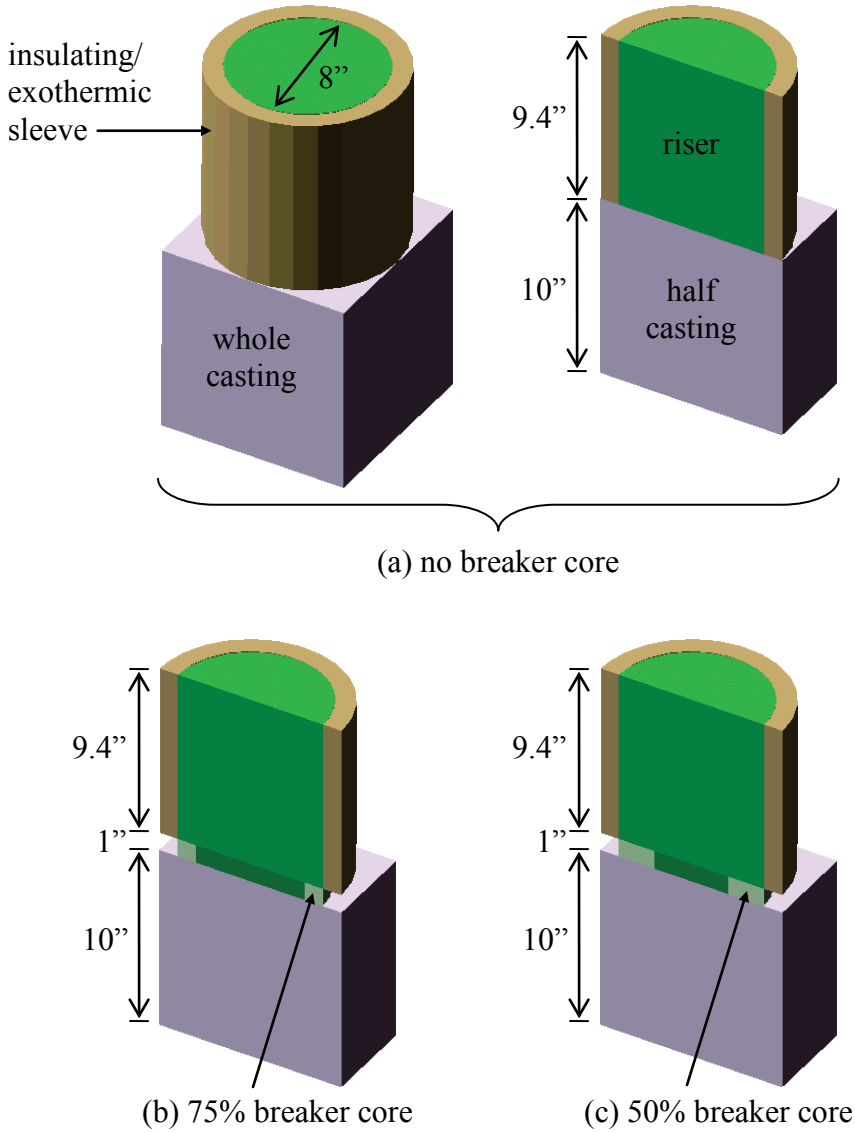


Figure 1. Schematics of cube castings with the three different riser arrangements considered in this study.

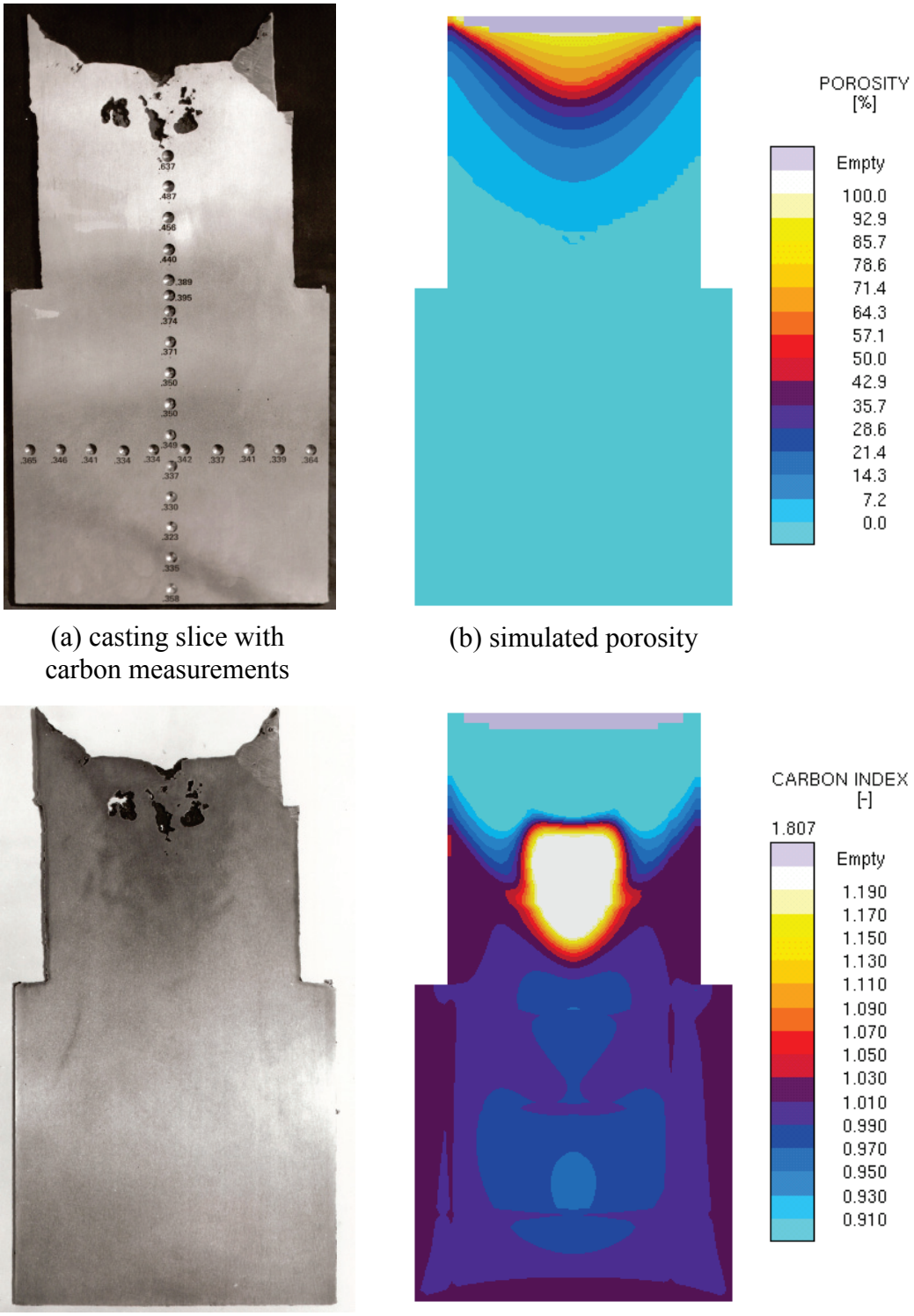


(a) casting slice with carbon measurements

(b) simulated porosity

(c) etched casting slice

(d) simulated C segregation

Figure 2. (a) Mid-casting slice of cube with no breaker core, showing carbon measurements; (b) porosity prediction at casting mid-plane from corresponding simulation; (c) etched mid-casting slice of cube with no breaker core, and (d) predicted carbon macrosegregation at casting mid-plane. Photographs courtesy of Ken Murphy. [2-4]

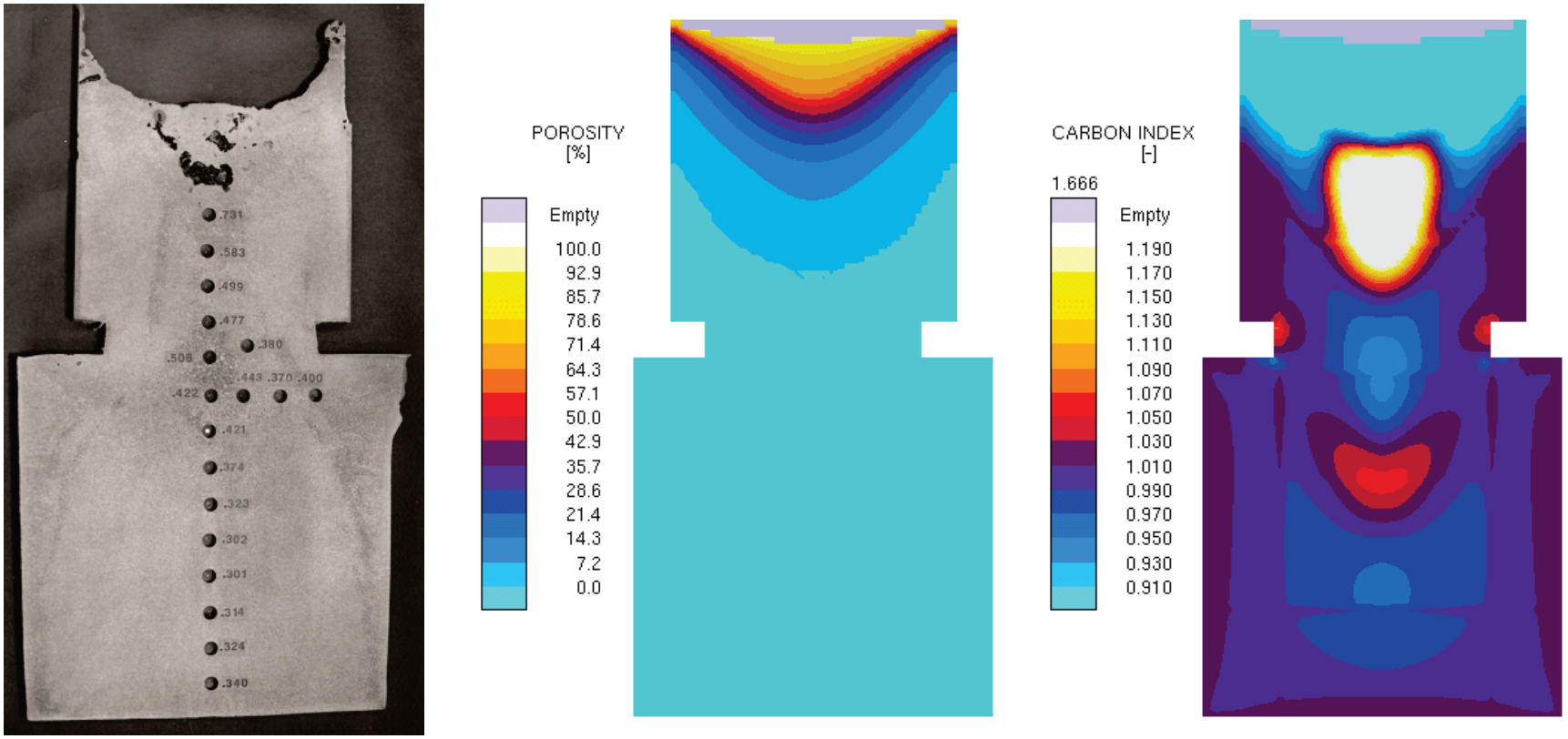


(a) casting slice (b) simulated porosity (c) simulated C segregation

Figure 3. Results for cube with 75% breaker core: (a) etched mid-casting slice, showing carbon measurements; simulated (b) porosity and (c) carbon segregation index results at the casting mid-plane. Photographs courtesy of Ken Murphy.[2-4]

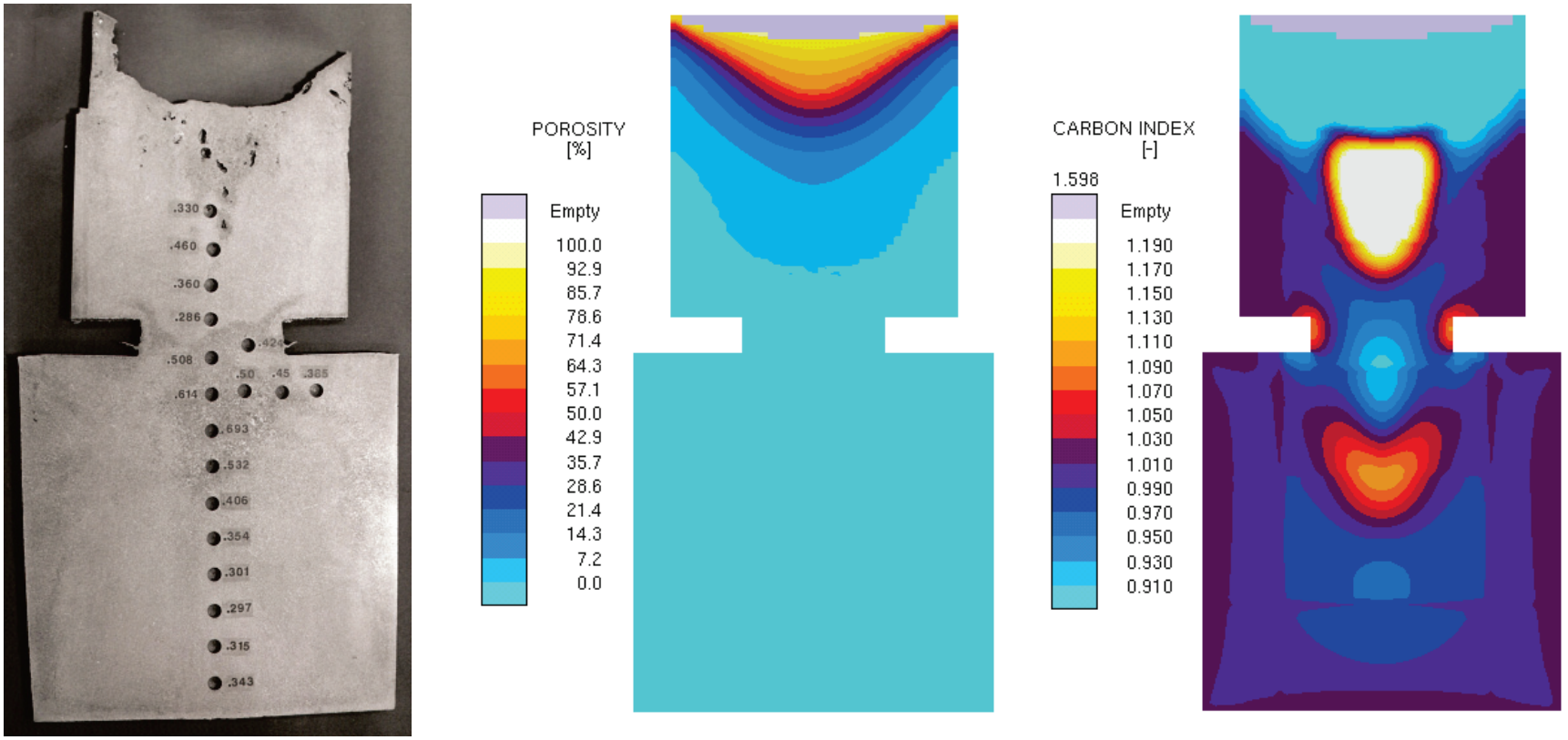


(a) casting slice (b) simulated porosity (c) simulated C segregation

Figure 4. Results for cube with 50% breaker core: (a) etched mid-casting slice, showing carbon measurements; simulated (b) porosity and (c) carbon segregation index results at the casting mid-plane. Photographs courtesy of Ken Murphy.[2-4]

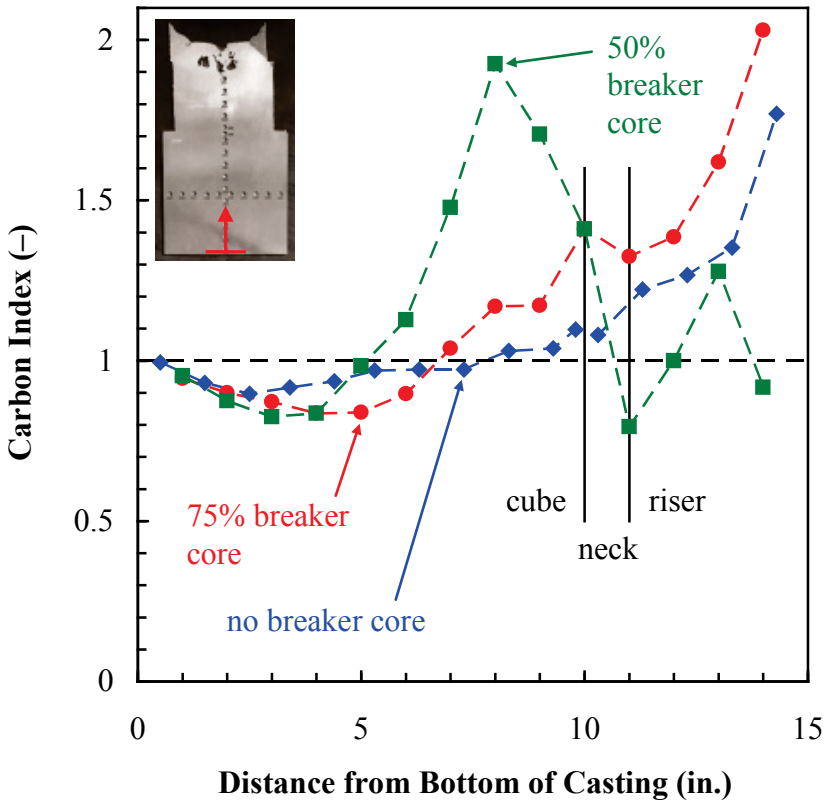


Figure 5. Measured vertical centerline carbon index values for casting without breaker core, as well as for castings with 75% and 50% breaker cores. Carbon index is computed by dividing the carbon measurements shown in Figs. 2a, 3a and 4a by the measured ladle carbon content, 0.36%.

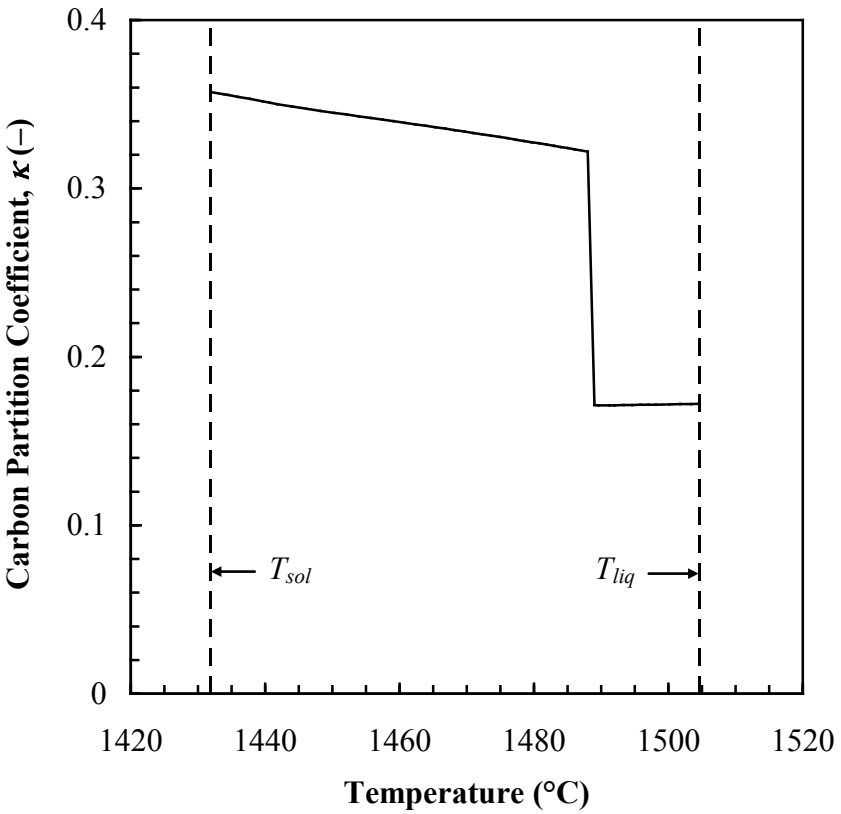


Figure 6. Temperature-dependent carbon partition coefficient curve for AISI 1035 steel.

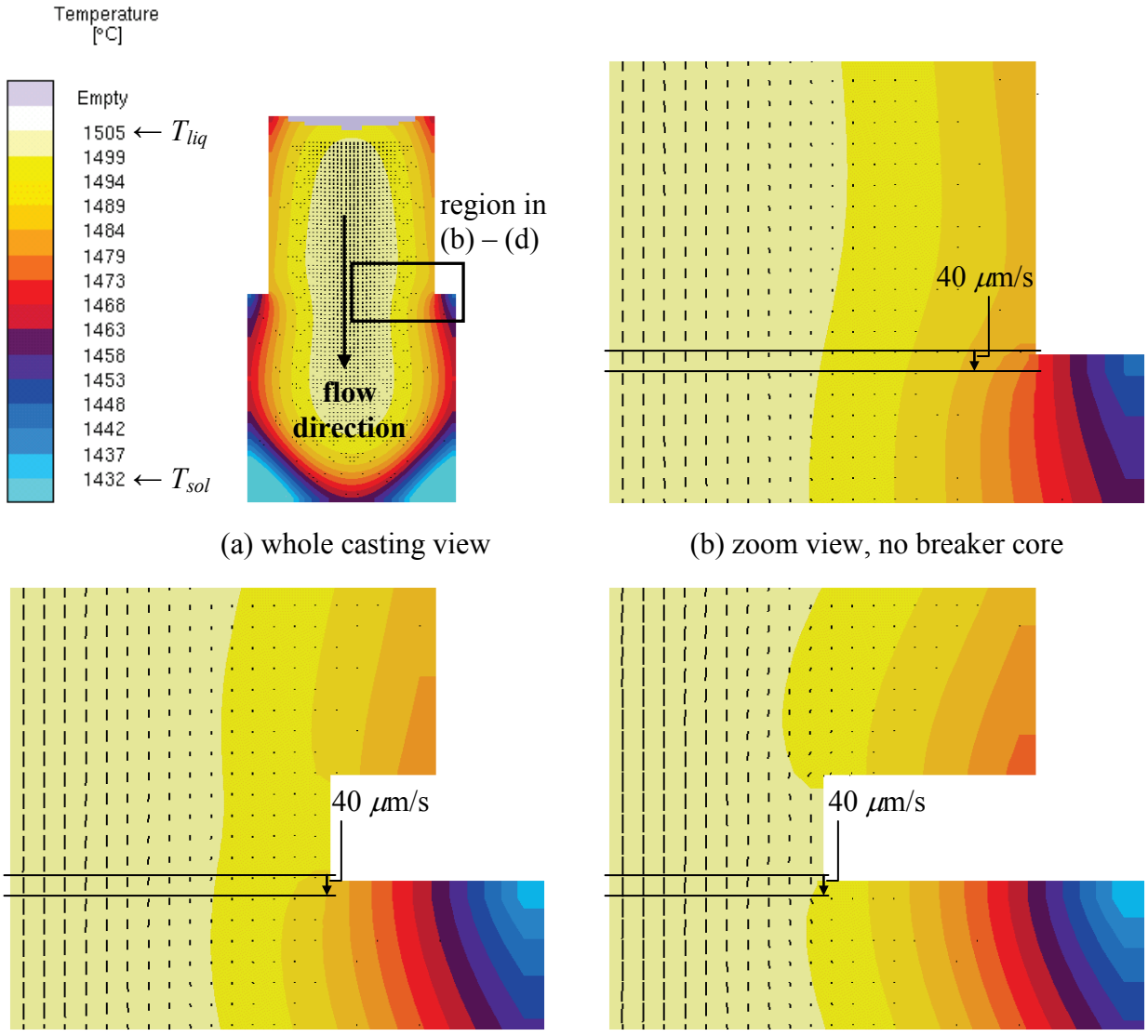


(a) whole casting view

(b) zoom view, no breaker core

(c) zoom view, 75% breaker core

(d) zoom view, 50% breaker core

Figure 7. Simulated velocity vectors shown at the casting mid-plane for all castings considered: (a) view showing the entire casting with no breaker core, indicating the flow direction and illustrating the region considered in (b) – (d).

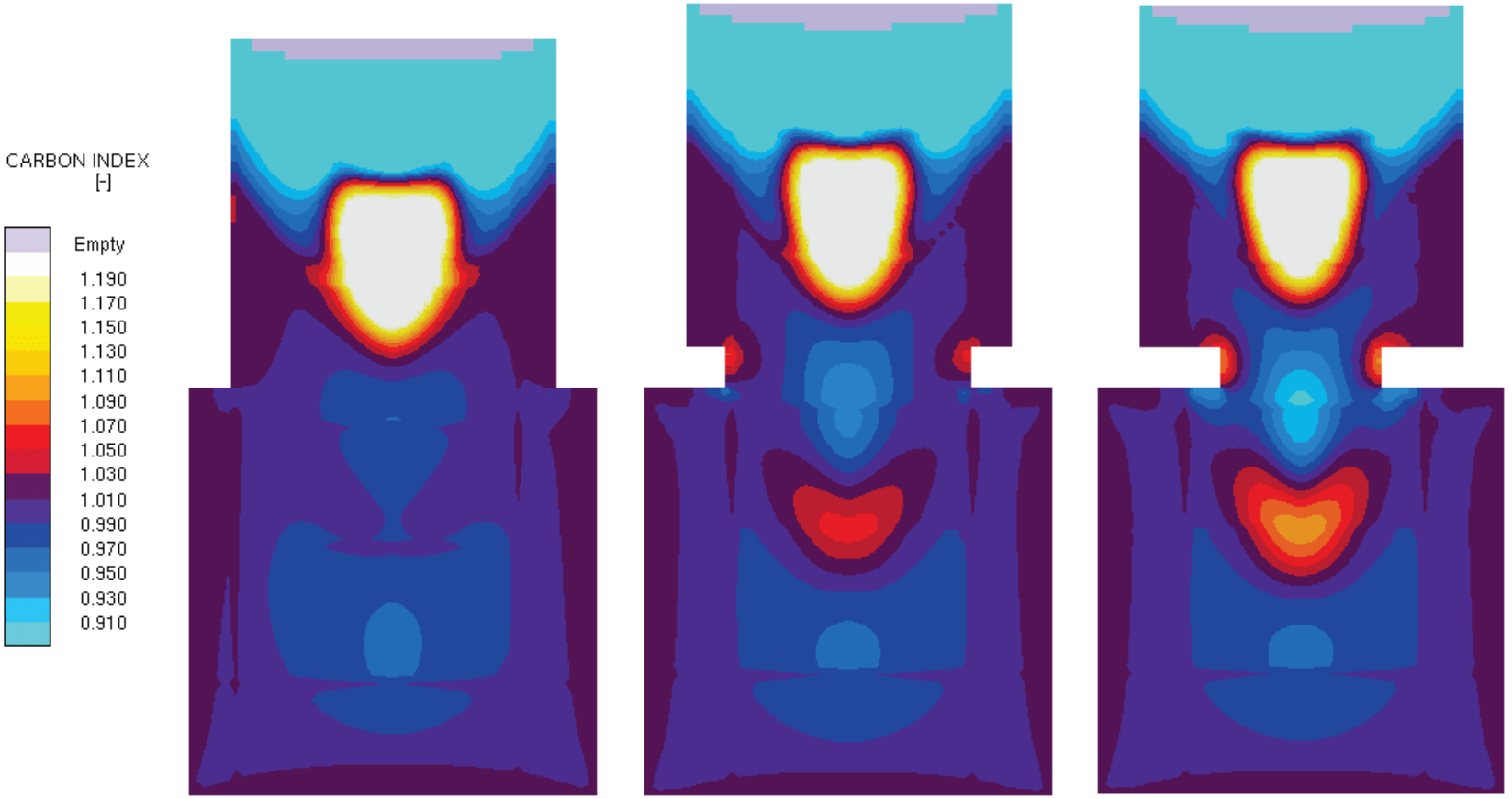


(a) no breaker core (b) 75% breaker core (c) 50% breaker core

Figure 8. Comparison of simulated mid-plane carbon index results.

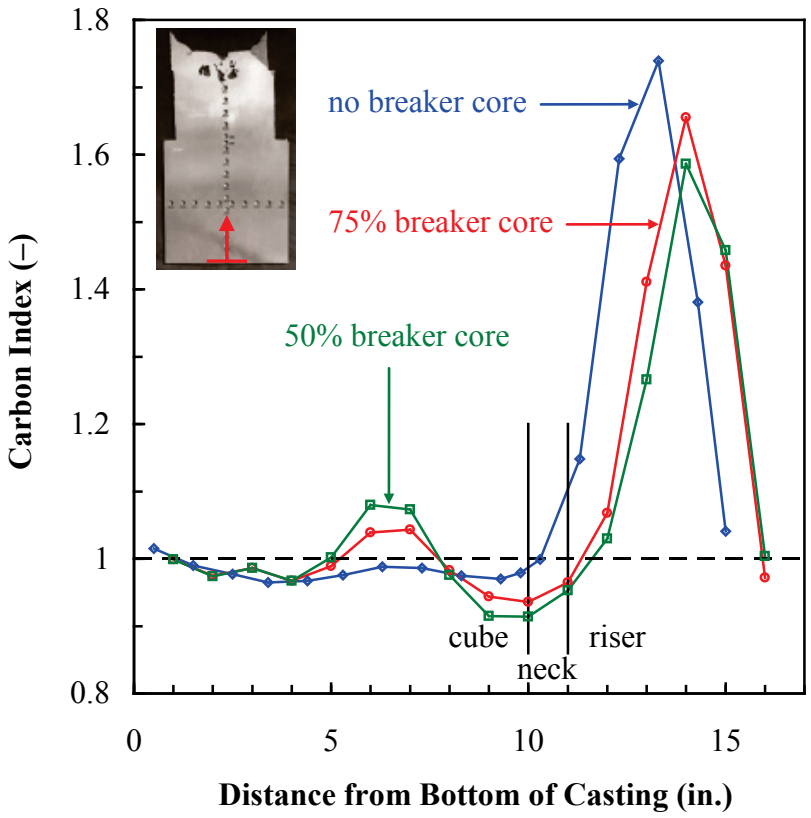


Figure 9. Comparison of simulated vertical centerline carbon index values for all castings considered.

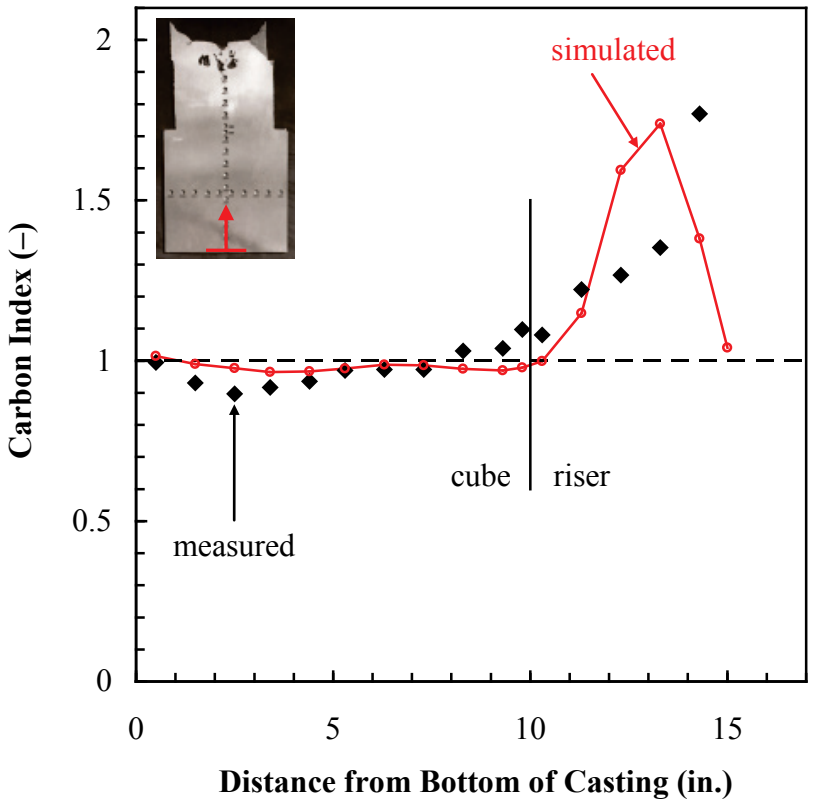


Figure 10. Measured and simulated vertical centerline carbon index values for casting without breaker core.

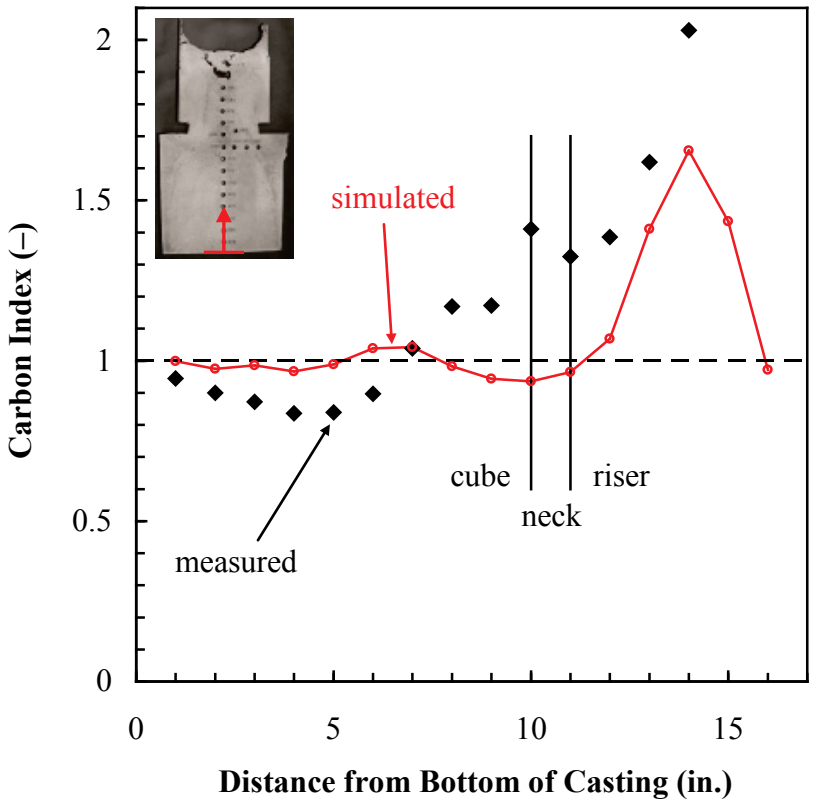


Figure 11. Measured and simulated vertical centerline carbon index values for casting with 75% breaker core.

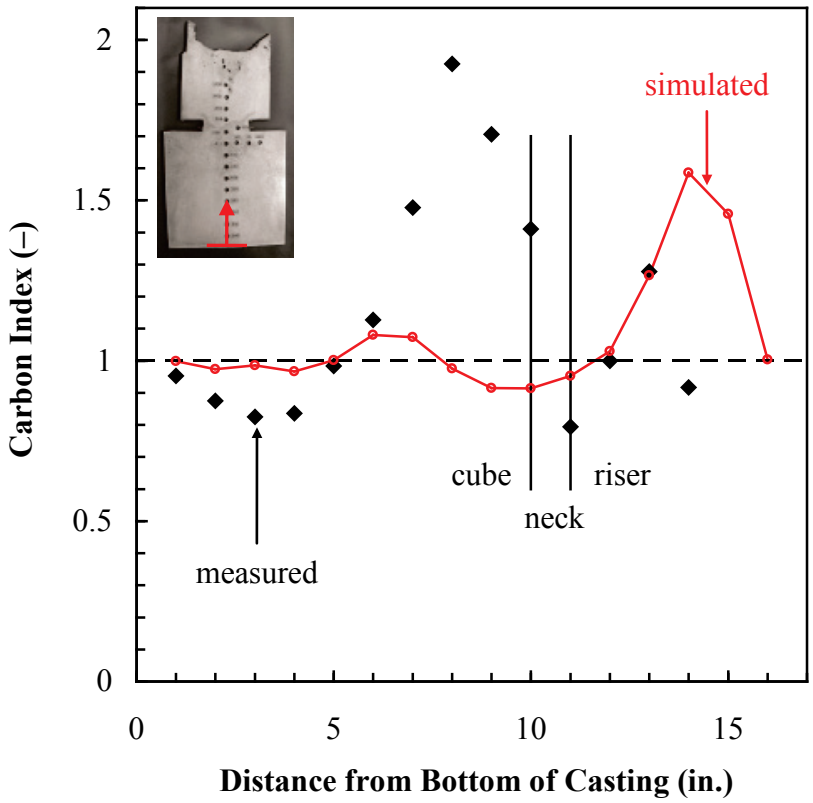


Figure 12. Measured and simulated vertical centerline carbon index values for casting with 50% breaker core.